Martinez Garzon, P., Heidbach, O., Bohnhoff, M. (2020): Contemporary stress and strain field in the Mediterranean from stress inversion of focal mechanisms and GPS data. - Tectonophysics, 774, 228286.

https://doi.org/10.1016/j.tecto.2019.228286

Contemporary stress and strain field in the Mediterranean from stress inversion of focal mechanisms and GPS data

Patricia Martínez-Garzón[a,*], Oliver Heidbach[a], Marco Bohnhoff[a,b]

[a] *Helmholtz Centre Potsdam, GFZ German Research Centre for Geosciences, Telegrafenberg, 14473 Potsdam, Germany*
[b] *Institute of Geological Sciences, Free University of Berlin, Berlin, Germany*

ARTICLEINFO

Keywords:
High resolution stress field orientation mapping
Plate tectonic forces
Mediterranean region
Maximum horizontal stress
Earthquake focal mechanisms
World stress Map

ABSTRACT

Mapping the contemporary stress field of the Mediterranean provides fundamental insights on the complexity of plate tectonic forces throughout the region and at different depths. Despite increased data availability and methodological improvements, most recent comprehensive stress field characterization across the entire Mediterranean dates back to 1995. To extend the regional stress information, we use all earthquake focal mechanisms compiled in the World Stress Map database release 2016 for a formal stress inversion. Our main goals are to (1) improve the resolution of the stress field orientation, (2) evaluate the performance of the recently refined stress inversion methodology in a tectonically complex region, (3) test the hypothesis of a depth-dependent stress orientation heterogeneity, and (4) compare different types of stress and strain observations from surface using the GPS-derived information on the strain rate tensor down to the seismogenic crust using summation of normalized seismic potencies. The obtained stress orientations generally capture the main seismotectonic features, including tectonically complex settings such as the Alpine Orogeny or the Ionian Sea. The orientation of the maximum horizontal stress S_{Hmax} tends to be uniform with depth within uncertainties while larger stress heterogeneity (quantified by means of the focal mechanism diversity and misfit angles) is found between 5 and 14 km. Both, the orientation of the largest horizontal shortening axis of the strain field from potency tensors, and horizontal strain rate tensor from GPS data are generally sub-parallel to S_{Hmax} orientation, indicating a linear stress/strain relationship and that the orientations of the co-seismic release and interseismic strain accumulation are generally consistent.

1. Introduction

Characterization of the contemporary crustal stress and strain fields and their relation across different tectonic settings provides fundamental insights on plate tectonic forces and the mechanics of faults (Richardson, 1992; Zoback, 1992; Scholz, 2002). The stress field is ultimately responsible for shaping the landscape, e.g. the growth of orogenic belts and extensional basins (e.g. Ghisetti, 2000; Cloetingh et al., 2007; Luttrell and Smith-Konter, 2017). Additionally, detailed knowledge of the stress field orientation allows to assess the slip potential of faults, therefore playing an important role in seismic hazard and risk assessment (e.g. Morris et al., 1996; Stein et al., 1997; Heidbach and Ben-Avraham, 2007; Vavryčuk, 2011; Walsh and Zoback, 2016; Martínez-Garzón et al., 2016a; Wollin et al., 2018).

Information about the contemporary stress and strain field can be inferred from different types of observations, each of them related with specific assumptions and conditions. The stress field orientation is largely derived from borehole data (borehole breakouts, drilling induced tensile fractures, hydro-fracs) and earthquake focal mechanisms. While borehole data are only available down to typically about five kilometers with very few exceptions, earthquake focal mechanisms are the most common indicator to sample the stress field orientation, typically throughout the seismogenic (upper crustal) layer, and - along subduction zones - down to uppermost mantle depth levels.

A global compilation of contemporary crustal stress information is provided by the World Stress Map (WSM) project that started in 1986 (Zoback et al., 1989; Zoback, 1992; Heidbach et al., 2010). The most recent WSM database release contains 42,870 data records, (Heidbach et al., 2018). In the past decade the stress pattern of several regions and countries has been revised and interpreted based on the WSM database and additional information (Bird et al., 2006; Hurd and Zoback, 2012; Carafa and Barba, 2013; Reiter et al., 2014; Assumpção et al., 2016; Hu et al., 2017; Rajabi et al., 2017). However, the complex stress pattern of the Mediterranean region has not been re-visited after the key papers from Müller et al. (1992), Rebaï et al. (1992) and Gölke and Coblentz (1996) although the number of data records in this region has increased by a factor of five since then. In particular, the number of reported earthquake focal mechanisms in the Mediterranean region grew to almost 5000, thus allowing to derive spatial stress field variations based on stress inversions in much greater detail. With this substantial increase in stress information it is now possible to extend the earlier work that focused on the long wave-length

* Corresponding author at: Helmholtz Centre Potsdam, GFZ German Research Centre for Geosciences, Section 4.2: Geomechanics and Scientific Drilling, Telegrafenberg, 14473 Potsdam, Germany.
E-mail address: patricia@gfz-potsdam.de (P. Martínez-Garzón).

pattern and its relation to the key tectonic forces that are driving this pattern. Furthermore, the advent of GPS in the past three decades offers the opportunity to compare contemporary stress and strain observations.

In this study, we revisit and extend the mapping of the contemporary stress field for the Mediterranean region using all focal mechanisms compiled in the WSM database release 2016 (Heidbach et al., 2018) for a formal stress inversion. Our main goals are to (1) resolve the stress field orientation for this region at a higher resolution and free of subjective parameters, (2) evaluate the performance of our stress inversion methodology in a tectonically complex region, (3) test the hypothesis of similar stress field orientations and heterogeneity with depth, and (4) compare the resulting stress pattern with the horizontal strain rate tensor derived from GPS measurements at the surface and with the co-seismic strain from the summation of seismic potencies in the brittle crust. The similarities and discrepancies between these observations and their tectonic implications are then evaluated and discussed.

The manuscript is structured as follows: In Section 2, we review the main seismotectonic features of the Mediterranean region from a compilation of key literature sources. In Section 3, we describe details of the applied stress inversion methodology as well as the characteristics of the employed dataset. In Section 4, we report on the main results of the mapping of the stress field orientation, which includes an average mapping over the entire depth range of the seismicity using a moving window approach sampling different depth ranges to detect potential stress rotations or changes in the stress regime, and a comparison with different stress indicators from the WSM. Within Section 5, we elaborate on the main stress and tectonic pattern observed for the Mediterranean region. In Section 6, we compare our stress inversion mapping with strain rate tensors in the different region as derived from GPS data and calculated potency tensors. Main conclusions are summarized in Section 7.

2. Seismotectonics of the Mediterranean region

Containing all three types of plate boundaries, the Mediterranean is one of the Earth's tectonically most complex regions (Fig. 1). The active tectonics of the Mediterranean region results in overall high seismicity and subsequent high seismic hazard both increasing from west to east (Grünthal and Wahlström, 2012; Giardini et al., 2014), in agreement with eastward enhanced strain rates (Kreemer et al., 2014). The highest cumulative seismic moment release is currently observed in the south Aegean/western Anatolian region, along the northern boundary of the Anatolian plate, along the Apennines in Italy and in northern Algeria (Fig. 2). Some of the main seismotectonic regions in the Mediterranean are summarized below:

(i) **Western Mediterranean region:** The present-day tectonic stress pattern in the western Mediterranean region is mostly transpressional mixing strike-slip and reverse faulting with an overall NWSE-trending S_{Hmax} orientation resulting from the Africa-Eurasia plate convergence, which is also in agreement with neotectonics stress indicators (e.g. Fernández-Ibáñez et al., 2007; Custódio et al., 2016; Soumaya et al., 2018). Recent studies combining geodetic and geological data showed that the current deformation pattern in this region is compatible with a slab dragging tectonics (Spakman et al., 2018). Small deviations from the average orientation could be related to steep gradients of crustal thickness variations in the region. In contrast to other orogenic regions such as the Alps, a fan-shaped pattern of S_{Hmax} perpendicular to the topography has not been recovered in the Alboran Sea.

(ii) **Alpine orogeny:** The overall agreement between different types of stress indicators in this region was first pointed out by Scheidegger (1981). Here, the prevailing S_{Hmax} orientation is perpendicular to the Alp orogenic arc resulting in a counterclockwise rotation of the S_{Hmax} pattern from East to West by approximately 40° (Reinecker et al., 2010). In this region, an overall good agreement exists between seismic and surface deformation (Houlié et al., 2018).

(iii) **Italian Peninsula:** The stress field over the Italian peninsula displays strong variations, including normal faulting stress regime in the central part along the Apennines and a first order rotation in the northern part following the structure of the Alpine orogeny. The southern section around Sicily and the Ionian Sea represents one of the most complex regions in the Mediterranean, potentially containing all three stress regimes (Montone et al., 2004). Pierdominici and Heidbach (2012) investigated the variability of the stress field with depth in Italy and adjacent regions and also elaborated on the wave-length of the stress pattern. Their results indicate a rather constant stress field orientation with depth, but short wave-lengths of the S_{Hmax} orientation pattern. The latter suggests that the stress field orientation is controlled by regional and local sources rather than by the first-order plate tectonics only.

(iv) **Aegean region:** The Aegean region has been the target of intense research due to its high seismicity and associated seismic hazard. Stress field mapping within the Aegean Sea reported a predominantly normal faulting stress regime with the S_1 axes mostly sub-vertical (Konstantinou et al., 2017) and a NS extension observed by GPS (Reilinger et al., 2006; Kreemer et al., 2014). This region including the Hellenic volcanic arc is dominated by the southward directed roll-back of the subduction zone of the towards Africa that results in a southward moving Aegean micro-plate with up to 30 mm/year with respect to a fixed European plate (Kreemer and Chamot-Rooke, 2004; McClusky et al., 2000). The convergence rate between the Aegean and African plates has been estimated to be 35 mm/yr (McClusky et al., 2003; Reilinger et al., 2006) and 33-34 mm/yr (Kreemer and Chamot-Rooke, 2004). The curved plate boundary along the Hellenic arc together with a uniform NNE-trending subduction below the Aegean-Anatolian domain results in a systematically varying angle between down-dip orientation of the oceanic lithosphere and the trend of the plate margin as derived

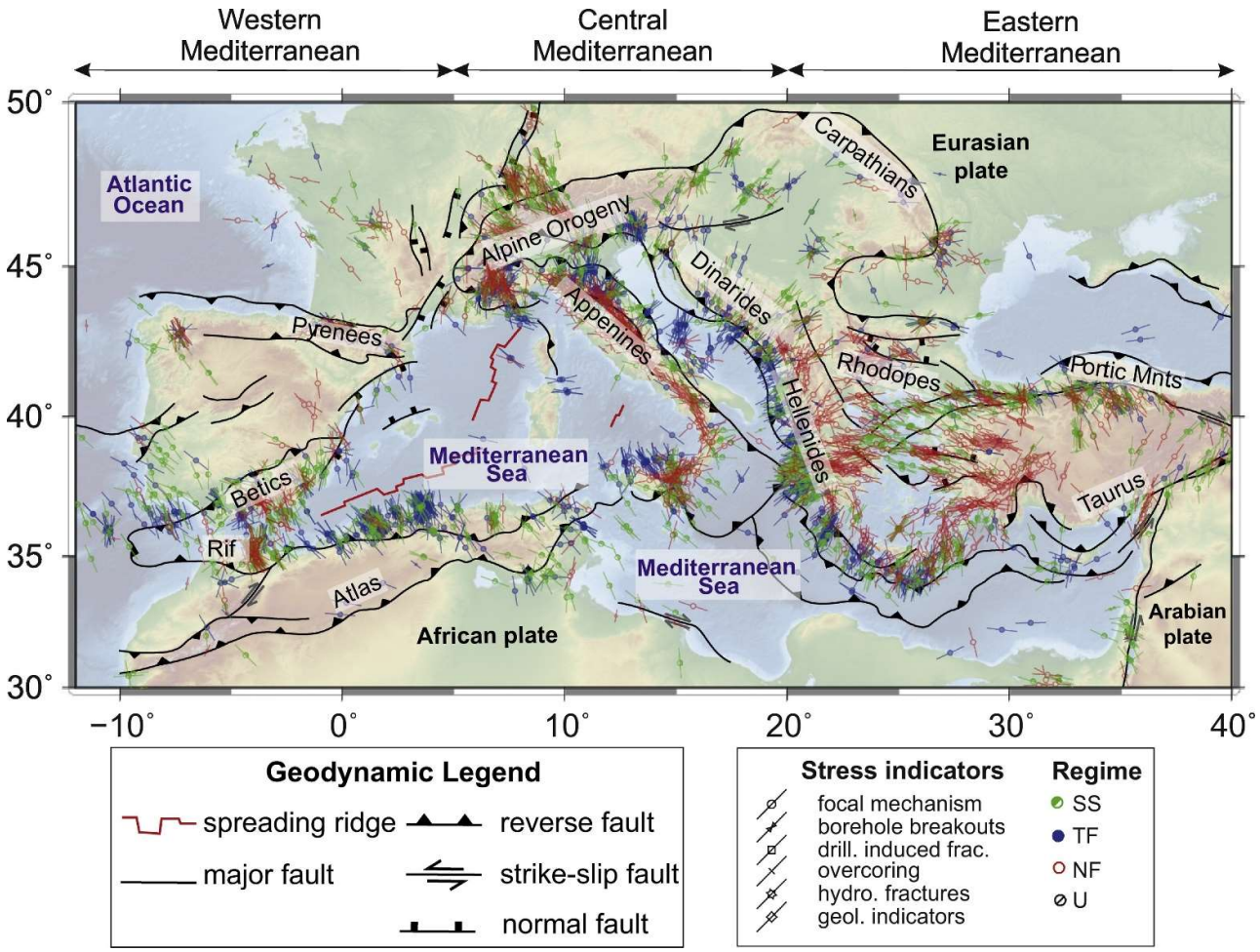

Figure 1. *Main geodynamic units and plate boundaries of the Mediterranean region as well as stress data with A-C quality from the WSM database release 2016 (Heidbach et al., 2018). Geodynamic data is compiled after Jolivet et al. (2009).*

from stress inversion of interpolate seismicity focal mechanisms (Bohnhoff et al., 2005).

(v) **Anatolian Plate:** The Anatolian Plate is laterally extruded by up to 25 mm/yr relative to Eurasia due to the collision of the Arabian plate with the Eurasian plate in the east and the roll-back of the Hellenic subduction zone and the consequent back-arc spreading of the Aegean Sea in the west (McClusky et al., 2000, 2003; Westaway, 1994; Heidbach and Drewes, 2003; Le Pichon and Kreemer, 2010; Bohnhoff et al., 2016). As a result, the Anatolian plate displays a westward motion combined with a counterclockwise rotation (Reilinger et al., 2006) and substantial NS extension at its western part. The stress field has been estimated for selected regions, in particular for the Sea of Marmara region due to the high seismic hazard and its implicit risk due to its vicinity of the Istanbul metropolitan area. A transtensional stress regime combining right-lateral strike-slip as along most part of the North Anatolian Fault Zone (NAFZ) and NS-oriented normal faulting appears to be predominant in this region and led to the opening of the Sea of Marmara as a pull-apart structure, however, with lateral changes of the stress pattern at relatively short spatial scales (Hergert and Heidbach, 2010; Örgülü, 2011; Wollin et al., 2018).

3. Stress inversion procedure and data processing

For first-order mapping of principal stress orientations and the stress regime, the P-, T- and B-axes of earthquake focal mechanisms could be used as proxies for the orientations of the principal stress axis (Zoback, 1992), however, with obvious limitations in reliability (Wallace, 1951; McKenzie, 1969; Célérier, 2010). Given this, the S_{Hmax} derived from these are assigned at best to C-quality according to the WSM quality ranking scheme indicating that they are only reliable to within ±25° (Zoback, 1992; Heidbach et al., 2010). To better constrain the stress orientations, an inversion of several focal mechanisms is used to derive the deviatoric stress tensor (e.g. Michael, 1984, 1987; Hardebeck and Hauksson, 2001). In contrast to borehole breakouts or individual focal mechanisms, stress inversion provides an integrated stress tensor sampling the entire region of all earthquakes used for the inversion. The output of the stress inversion are the orientations of the three principal stresses and the stress ratio R:

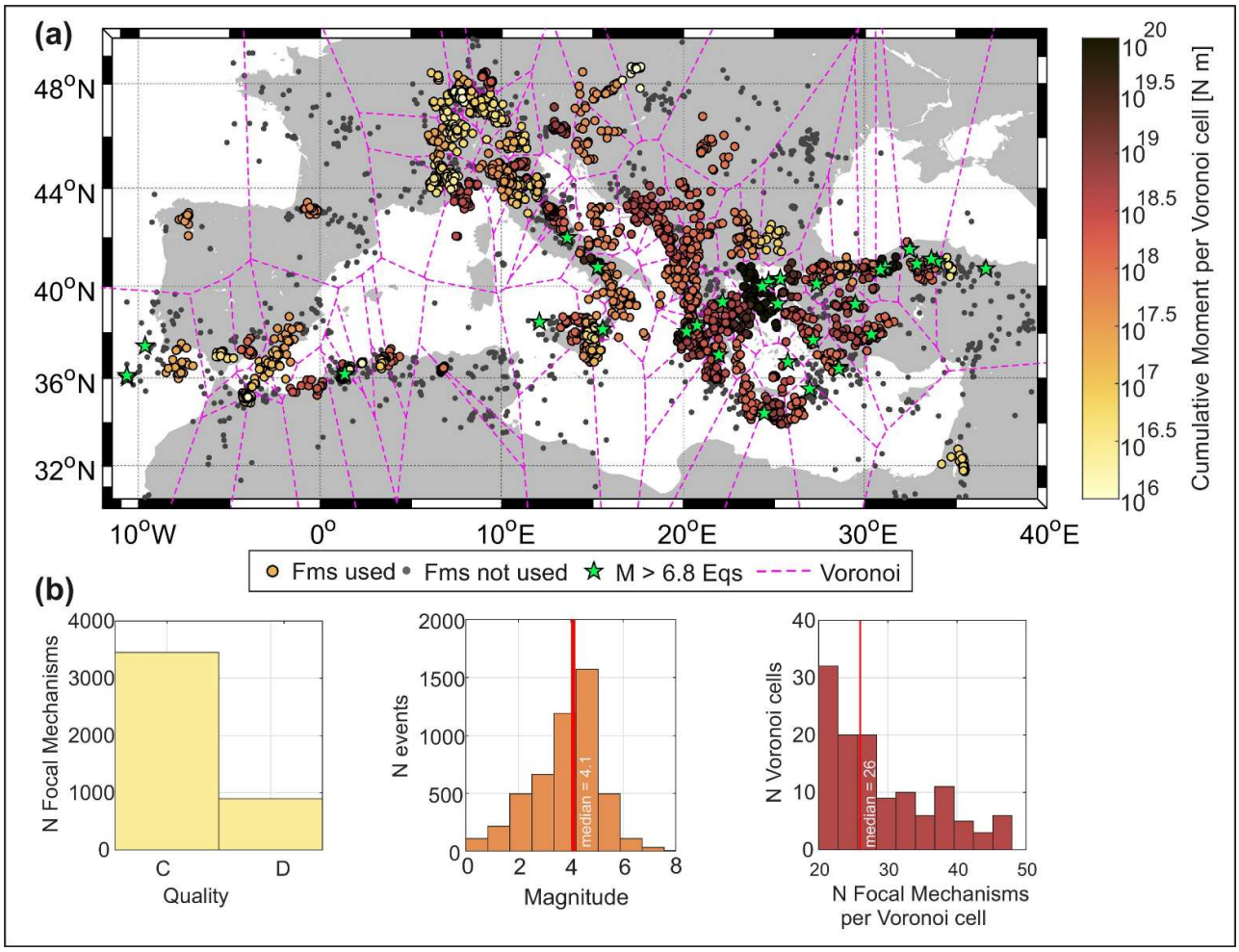

Figure 2. *(a) Input seismic data color encoded with the cumulative moment release of all earthquakes contained in the corresponding Voronoi cell (stress region). Grey dots represent seismic events rejected during the grouping process. Green stars mark the earthquakes with $M > 6.8$ contained in the catalog. Purple lines denote the different Voronoi cells (stress regions) obtained in the grouping procedure. (b) Histograms displaying different statistics of the input data. From left to right: Quality of focal mechanisms, magnitude-frequency distribution of the employed seismicity and number of focal mechanisms per stress region. (For interpretation of the references to color in this figure legend, the reader is referred to the web version of this article.)*

$$R = \frac{\sigma_1 - \sigma_2}{\sigma_1 - \sigma_3} \quad (1)$$

where σ_1, σ_2 and σ_3 represent the three principal stresses, from most to least compressive.

Even though the WSM database has compiled almost 5000 focal mechanisms in the Mediterranean area, only 91 data records from stress inversions from regional studies are included (e.g., Frepoli and Amato, 2000; Kiratzi, 2002; Kastrup et al., 2004; Bohnhoff et al., 2005; Ousadou et al., 2014). However, an analysis using a technically consistent and modern stress inversion for the entire Mediterranean that includes the entire set of available focal mechanisms has not yet been performed and is the backbone of this study. We focus our analysis on the area within the geographical coordinates: 30°/50° North and -12°/40° East (Fig. 1). We employ all 4886 focal mechanisms available within this region from the WSM database release 2016 with earthquake magnitudes ranging between 0.4 and 8.0 (Figs. 1, 2a). This focal mechanism catalog is unconventional in the sense that it consists of different sub-catalogues with different magnitudes of completeness. The median magnitude of the earthquakes in the catalog is M 4.1 and the dataset covers the entire instrumental time period from 1908 to 2016 (Fig. 2b).

Within the WSM database, the quality of the stress field orientation derived from a single focal mechanism is assigned according to the magnitude of the corresponding event, with Quality C corresponding to events with magnitude $M \geq 2.5$ and Quality D corresponding to smaller earthquake magnitudes. About 85% of employed seismic events correspond to quality C, which is associated with a stress field orientation uncertainty of about 25 degrees (Fig. 2b).

The focal mechanisms need to be grouped into subdomains for the subsequent inversion for the deviatoric stress tensor. Therefore, the focal mechanisms from the WSM were spatially grouped by us employing an objective iterative technique based on a k-means algorithm (see Martínez-Garzón et al., 2016b, for details). In this technique, the only parameter to be set is the minimum number of focal mechanisms per region. This parameter is selected based on a number of synthetic tests performed to achieve a resolution of the stress tensor of

about 10° (Martínez-Garzón et al., 2016b). In the first step, the algorithm performs an objective splitting of the focal mechanisms based on the maximization of the silhouette coefficient. In the next step, each of the groups obtained from the preferred data discretization is further subdivided into smaller regions until the desired amount of focal mechanisms per domain is achieved. This way, each of the groups of focal mechanisms corresponds to one Voronoi cell region (see purple lines in Fig. 2a).

Assuming a generic uncertainty of individual focal mechanisms of about ~20°, previous synthetic tests have shown that about 30 focal mechanisms that sample different orientations are appropriate as a minimum for constraining the deviatoric stress tensor (Martínez-Garzón et al., 2016b). Therefore, the here obtained domains contain between 20 and 50 (median: 26) focal mechanisms (Fig. 2b). It is also important to quantify the focal mechanism variability contained in each group. In this case, we estimated the focal mechanism variability as the 3D rotation angle (Kagan, 1991) between each pair of focal mechanisms within a domain, and then calculate the median of the distribution. This way, we obtained that the focal mechanism diversity of our employed groups varies between 30 and 80 (median: 59) degrees.

Once the data was grouped, we performed the formal deviatoric stress tensor inversion for each group. We followed the stress inversion methodology proposed by (Martínez-Garzón et al., 2016b). The inversion employed is a refined and upgraded version of MSATSI (Martínez-Garzón et al., 2014) which is subsequently refined from the SATSI algorithm (Hardebeck and Michael, 2006). First, each of the focal mechanism groups is inverted independently for the deviatoric stress tensor following the iterative approach proposed by (Vavryčuk, 2014). Within this approach, out of the two fault planes available in each focal mechanism, we select the fault plane best oriented for failure within the recovered stress field orientation. The proximity of the corresponding fault plane to the optimally oriented fault plane within the given stress field is estimated by using the instability coefficient (Vavryčuk,

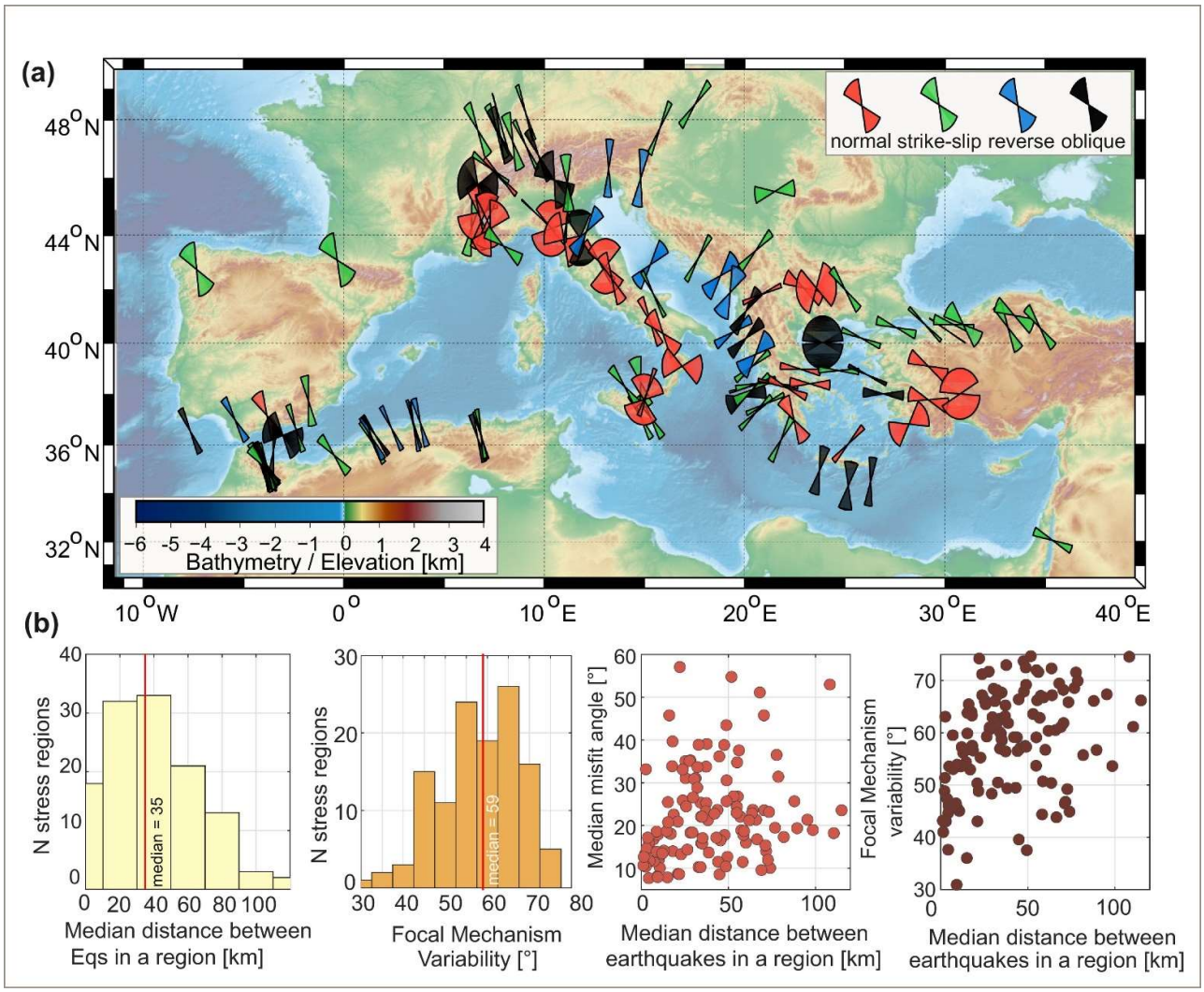

Figure 3. *Mapping of S_{Hmax} orientation in the Mediterranean region. The fan-shaped symbol indicates the 95% confidence interval of S_{Hmax} orientation, color encoded with the corresponding stress regime (red: normal, green: strike-slip, blue: reverse, black: oblique). (b) Different statistics, from left to right: median distance between pairs of earthquakes from each stress region, focal mechanism variability within each stress region quantified as 3D rotation angle (Kagan, 1991), and median distance between earthquake epicenters in each stress region vs median misfit from stress inversion and focal mechanism variability. (For interpretation of the references to color in this figure legend, the reader is referred to the web version of this article.)*

2011) which is defined as:

$$I = \frac{\tau - \mu(\sigma - \sigma_1)}{\tau_c - \mu(\sigma_C - \sigma_1)} \quad (2)$$

where τ and σ represent the shear and normal stresses on the fault plane, μ represents the friction coefficient and the subindex C refers to the optimally oriented fault plane within that particular stress field. $I = 1$ and $I = 0$ represent the optimal and worst orientation for failure, respectively. In this approach, a coefficient of friction needs to be assumed. We then performed a grid search in which we tested for each group a friction coefficient varying between 0.1 and 1 in steps of 0.1. For each group, we selected the friction coefficient that maximizes the overall instability of the fault planes contained within the corresponding group. Nevertheless, small changes in the friction coefficient are not observed to significantly modify the obtained results.

Once the most unstable fault plane out of each focal mechanism has been selected and the optimal friction coefficients have been obtained, we performed the final stress inversion for each grid according to these values. The S_{Hmax} orientation is then calculated from the stress inversion result following Lund and Townend (2007). Uncertainty of the stress field orientation and related parameters is calculated by bootstrap resampling of the focal mechanisms within each group (Michael, 1987). The consistency between the retrieved principal stress axis and the input focal mechanism data is evaluated by means of the misfit angleβ between the slip vector $\vec{s}$ and the shear traction vector$\vec{\tau}$ on the nodal plane selected by the highest instability coefficient:

$$\cos\beta = \frac{\vec{s} \cdot \vec{\tau}}{|\vec{s}||\vec{\tau}|}. \quad (3)$$

This parameter can be used to test the hypothesis of stress homogeneity within a certain region, or, alternatively, how heterogeneous the stress field from a certain region may be. In addition, we calculated the A_φ parameter (Simpson, 1997) for each inversion. This parameter provides a continuous scale for the stress regime. It is basically a combination of the Andersonian faulting regime index n (Anderson, 1905) and the stress ratio R and it is defined as:

$$A_\varphi = (n + 0.5) + (-1)^n \cdot (R - 0.5). \quad (4)$$

The integer n is set to 0 for normal faulting, 1 for strike-slip and 2 for reverse faulting. An A_φ value of 0.5 represents pure normal faulting, 1.5 is strike-slip and 2.5 pure reverse faulting.

While the methodological focus of this study is on the formal stress inversion of the entire dataset considering all seismicity available with depth < 30 km, in Section 4.2 we also investigated the variability of the stress field orientation with depth. To do so, an additional set of 12 stress inversions was performed. The inversions were performed including seismicity from 10 km depth intervals, moving in steps of 2 km. The peak of seismicity at 10 km depth was removed from these inversions to avoid using events with lower hypocentral depth quality (see details in Section 4.2). For each of these subsets, we followed a spatial data grouping and a formal stress tensor inversion as described above for the entire dataset.

4. Results

4.1. Principal stress orientations from stress inversion

Applying the grouping technique to the set of focal mechanisms from the Mediterranean region described in Section 3, we obtained 122 stress regions for which we resolved the stress tensor orientation, the stress ratio R and the orientation of S_{Hmax} (Fig. 3a). The S_{Hmax} orientation together with 95% confidence intervals and other stress-related parameters derived for each of the regions are provided in Table S1.

Fig. 3a shows the orientation of the maximum horizontal stress in each region derived from the formal stress inversion. The obtained stress field resolution reproduces correctly the main tectonic features and stress provinces. As a first order feature, the S_{Hmax} orientation of adjacent domains appears to be consistent in the majority of the explored areas (e.g. western Mediterranean), even when the results were calculated without introducing any damping factor. However, our stress mapping is also capable of capturing stress heterogeneities such as sharp variations of S_{Hmax} or changes in the stress regime within short distances. These are primarily observed in highly complex regions such as around Sicily or in the Alpine orogeny. In Fig. 3a, the stress regime (i.e. normal, strike-slip, reverse and oblique faulting) of each stress region is encoded with color of the fan-shaped symbol following the stress regime assignment of Zoback (1992). About 43% of the analyzed stress regions display strike-slip stress regime, while 25% display normal faulting and only 12% of the resolved areas display a reverse stress regime. The remaining areas (20%) display a mixed stress style.

To estimate the size of the region for which the resolved stress field orientation is representative, we estimated the median distance between each pair of earthquakes contained within a stress region. This measure is preferred over the area of the corresponding region, as sometimes the employed earthquakes are substantially more clustered in space. The median distances between pairs of earthquakes within the employed stress regions range between 0 and 120 (median: 35) km (Fig. 3b).

The focal mechanism diversity tends to increase with the size of the stress region (Fig. 3b). However, a number of regions of relatively small size are found to display large focal mechanism diversity. The median misfit angle β (Eq. (3)) is often used as a measure of the stress heterogeneity. In general, the median misfit angle tends to increase with median distance between pairs of earthquakes within a region (Fig. 3b), although this relation is not unambiguous.

In agreement with the different tectonic patterns of the Mediterranean region, a variation in the diversity of S_{Hmax} is observed, with a generally higher diversity in the central part of the analyzed region. In the western Mediterranean, (Lon < 5°E), the average and standard devia-

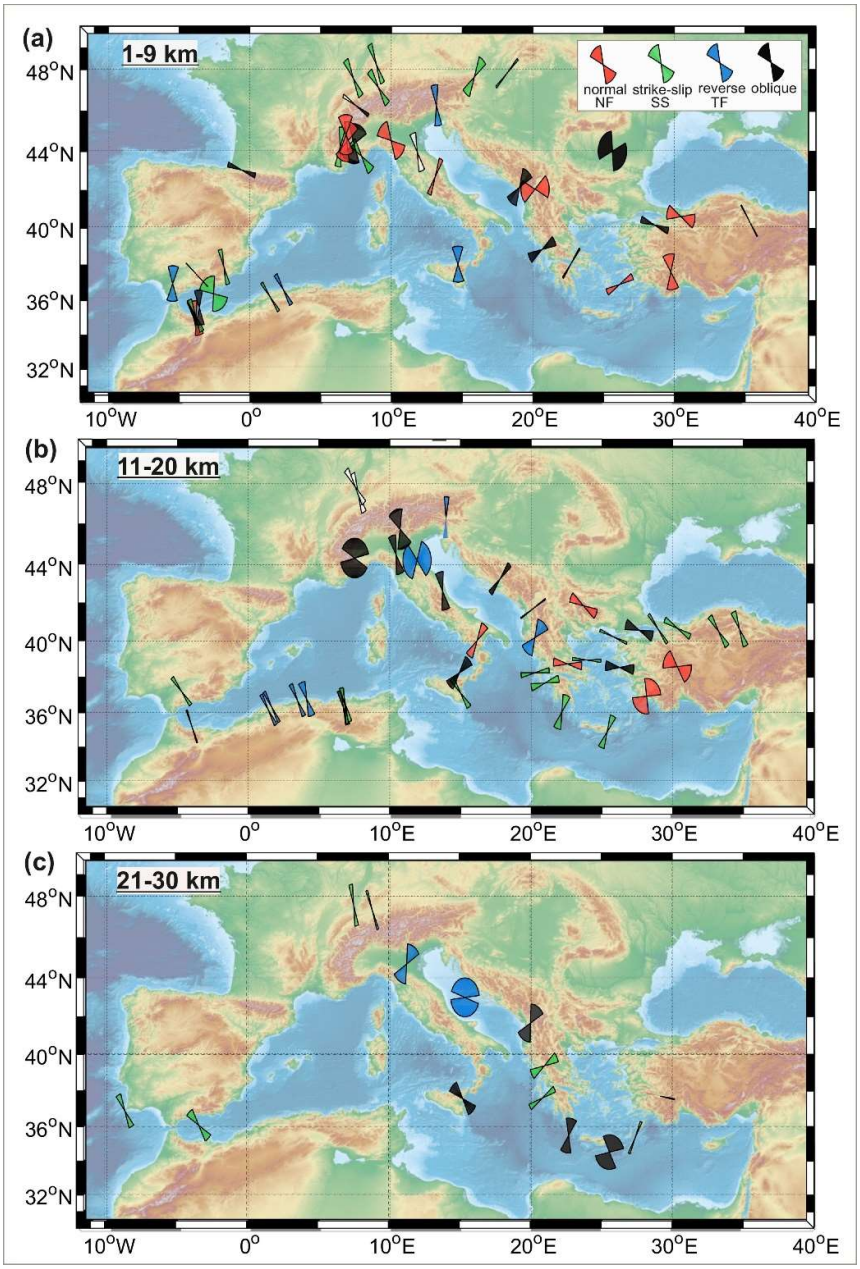

Figure 4. *Mapping of S_{Hmax} orientation in the Mediterranean region utilizing the seismicity from different depth intervals (a) 1-9 km, (b) 11-20 km, (c) 21-30 km. Symbols and color meaning is analogous as in Fig. 3.*

tion of the S_{Hmax} orientation is 146° and 31°, respectively.

In the central Mediterranean (6°E < Lon < 23°E), these values are 96° and 53°. Finally, in the eastern part of the study region, the average S_{Hmax} and standard deviation are 96° and 39°, respectively.

4.2. Variations of stress inversion results with depth

To evaluate the uniformity of S_{Hmax} with depth in the Mediterranean region, we applied the stress inversion methodology to a series of moving depth window inversions covering a depth range of 10 km each, and moving in depth steps of 2 km. As the WSM database 2016 does not include an estimation of the depth uncertainty of each individual event, we used 10 km depth intervals assuming an average depth uncertainty of ±5 km. Nevertheless, a large number of earthquakes from the WSM database catalog display a hypocentral depth of 10 km (typical starting depth during hypocenter inversion, see Fig. S1 for a depth distribution of the events from the catalog). For this reason, all events with a hypocentral depth of precisely 10 km have been removed in these inversions. Three of these inversions are shown in Fig. 4, corresponding to depth intervals of [1-9] km (Fig. 4a), [11–20] km (Fig. 4b) and [21–30] km (Fig. 4c). These three layers contain 40, 41 and 14 individual stress inversions, respectively (Fig. 4).

To evaluate the variability in S_{Hmax} orientation with depth along the analyzed region, we selected areas of 1° by 1° and estimated the standard deviation of S_{Hmax} from

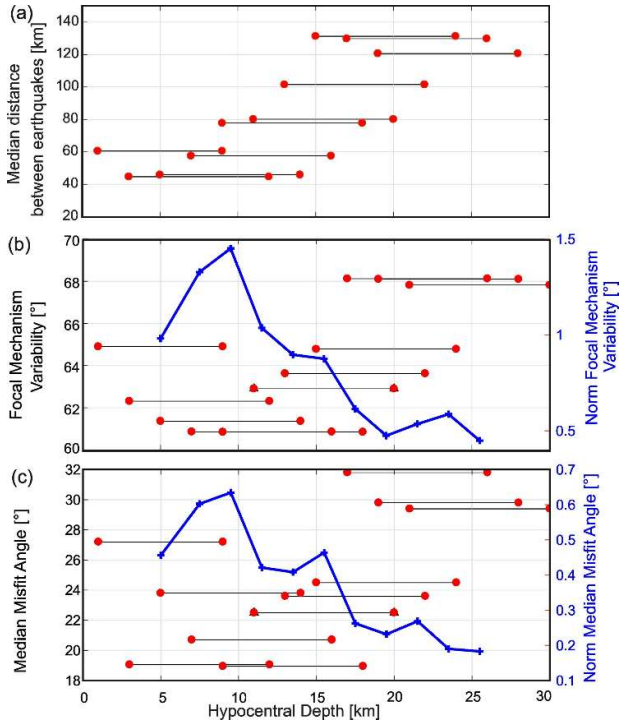

Figure 5. *Summary of parameters from the inversions performed sampling different depth intervals. (a) Median distance between earthquake pairs. (b) Median focal mechanisms variability (black lines with red circles on the extremes showing the sampling depth interval) and median focal mechanisms variability normalized by the corresponding median distance between earthquakes shown in (a) (blue line). In this case the hypocentral depth is taken as the mean of the sampled interval. (c) Same as (b) but for the median misfit angles. (For interpretation of the references to color in this figure legend, the reader is referred to the web version of this article.)*

all the stress inversions of different depths contained within each of these 1° by 1° areas (Fig. S2). The largest depth-dependent variability of S_{Hmax} orientation quantified as largest standard deviation between the stress inversions in that area are found in northern Italian Peninsula, east and west extremes of the Alpine orogeny, and small regions in northern Sicily-Messina Strait and within the Alboran Sea near Spanish coast (Fig. S2b).

The proportion of each stress regime is generally preserved within the different examined depth ranges. As the magnitude of the vertical stress increases with depth, a larger proportion of normal faulting with depth could be expected (Brudy et al., 1997). However, this change from reverse or strike-slip to normal stress has been observed to occur around the upper 4 km depth, which is beyond the resolution achieved here based on limited depth resolution of the earthquake hypocenters. The most notorious change here observed is an increase in the amount of oblique faulting in the 21-30 km depth range, from 19% of the stress inversions displaying oblique faulting within the 11-20 km depth range to up to 50% of oblique faulting in the 21-30 km depth range. Within the Mediterranean region, the seismicity from this depth interval is mainly related to subduction zones (e.g. the Hellenic arc and selected areas of the Ionian Sea, see Fig. 4c). Therefore, this oblique faulting at 21-30 km depth could be related to the seismicity occurring in the subduction plane.

We then compared the statistics of several stress-related parameters from the stress inversion distributions at the three representative depth ranges from Fig. 4 utilizing all the moving-depth window stress inversions performed. The distance between pairs of earthquakes from the same stress region, representing the size of the sampled area in each stress inversion significantly increases with depth, from a median value of 42 km in the 0-9 km depth range, to 80 in the depth range 11-20 km and up to 130 km in the 21-30 km depth range (Fig. 5a). Despite the smaller sampled areas, the focal mechanism diversity is comparable at 1-9 km depth than at 11-20 km depth (Fig. 5b). When we normalize the focal mechanism variability by the corresponding area of the represented region, a decreasing trend of the normalized focal mechanism variability is observed, reaching its maximum within the interval 5-14 km depth and decreasing with depth, illustrating a higher stress heterogeneity in this shallower portion of the crust (Fig. 5b). A similar effect is observed for the median misfit angles β, where misfit values are generally comparable despite of the larger differences in

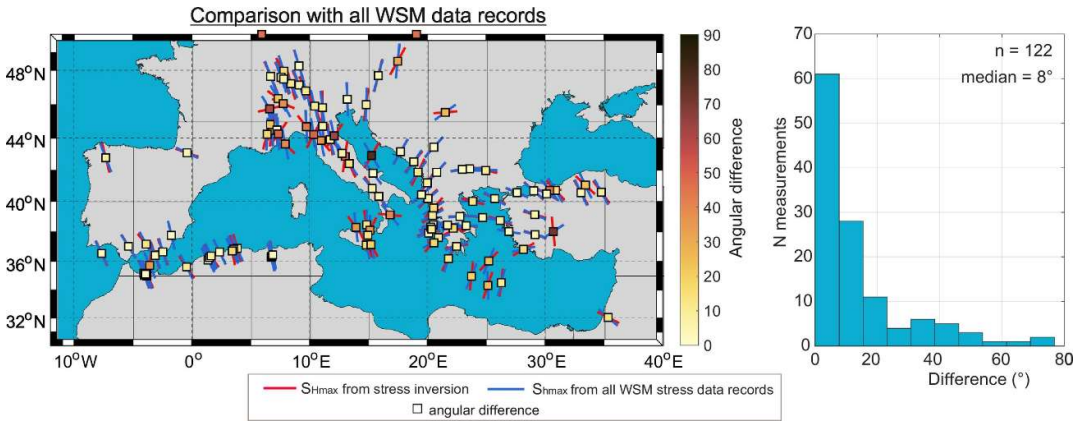

Figure 6. *Comparison of stress inversions obtained in this study with stress data records from WSM database release 2016. Left: S_{Hmax} from stress tensor inversions (red lines) together with the mean S_{Hmax} estimation using stress2grid v1.1 (Ziegler and Heidbach, 2019) and all WSM stress data records with A-C quality (dark blue lines). Right: Histogram of the differences between the mean S_{Hmax} estimate and the results from the stress inversion. Square symbols are color encoded with the angular difference between both. (For interpretation of the references to color in this figure legend, the reader is referred to the web version of this article.)*

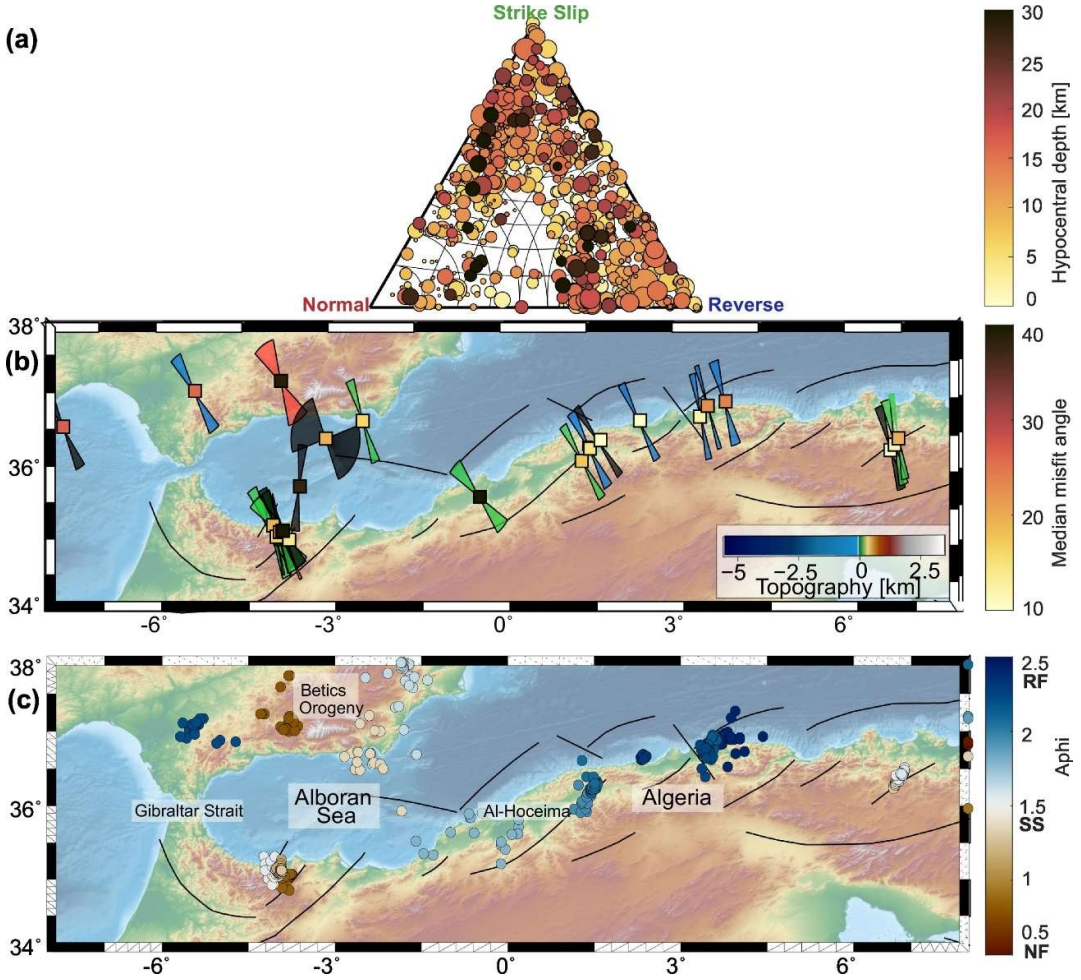

Figure 7. *Detailed stress pattern of the western Mediterranean region. (a) Ternary diagram showing the input focal mechanisms from the western Mediterranean region color encoded with hypocentral depth. (b) Recovered orientations of the maximum horizontal compressive stress S_{Hmax}. The width of the fan shapes indicates 95% confidence interval. Color of fan shapes is encoded with stress regime (red: normal, green: strike-slip, blue: reverse, black: oblique). The square in the center is color encoded with the median misfit angle β (see Eq. (3)). (c) Seismicity enclosed in each stress region, color encoded with the Aφ parameter for the corresponding region (0.5: normal faulting, 1.5: strike-slip, 2.5: reverse). Oblique stress regions are not included in the A_{φ} mapping. (For interpretation of the references to color in this figure legend, the reader is referred to the web version of this article.)*

the sampled area. However, when we normalize by the distance between earthquakes in the corresponding area, again we observed a maximum in the normalized misfit angle starting at the depth interval 5-14 km and generally decreasing with depth (Fig. 5c).

In summary, an overall consistency of the S_{Hmax} orientation with depth is observed. However, larger focal mechanism diversity and misfit angles β normalized by the area covered in each stress inversion suggests the largest stress heterogeneity within the depth interval 5-14 km and a trend towards decreasing afterwards.

4.3. Consistency between stress inversion and WSM stress data records

In the following, we compare our stress inversion results from Section 4.1 with the data records from the WSM database 2016. We estimate the mean S_{Hmax} orientation on a regular 0.1° grid using the Tool *stress2grid* v1.1 from Ziegler and Heidbach (2019) where a weight according to distance and data quality is set. We fix the search radius to 250 km for each grid point and use all WSM 2016 data records with A-C quality. For the comparison the nearest mean S_{Hmax} orientation from the grid to the centroid of the Voronoi cell is picked.

We generally observe a very good agreement between this realization and our result from the stress inversion with a median difference of only 8° (Fig. 6). This is not surprising, since the largest proportion of stress data records originate from earthquake focal mechanisms (Heidbach et al., 2018), which were here used as our input data for the inversion. Two isolated stress inversion results near the Adriatic Sea and the southwestern portion of the North Anatolian fault display large discrepancies. In addition, the western portion of the Alpine orogeny appears to display increased differences between the two estimations over a large area. This could indicate a larger heterogeneity of the stress field in this region, with different stress indicators providing non-consistent results.

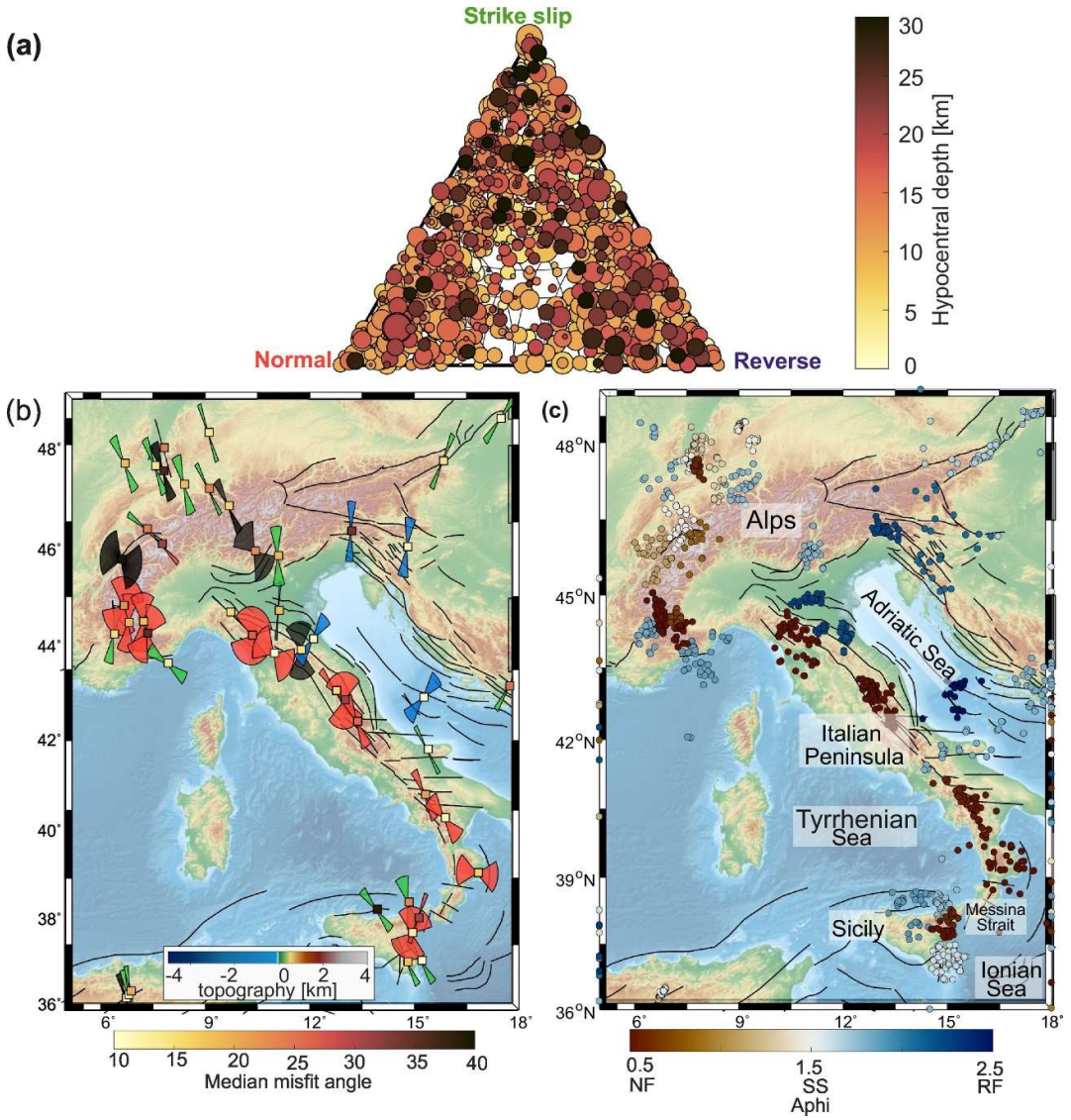

Figure 8. *Same as Fig. 7 but for central Mediterranean region.*

5. Stress and tectonic pattern of individual Mediterranean regions

In the following, we utilize our mapping of stress parameters to elaborate on the seismotectonic setting of selected regions where data coverage is sufficiently high:

5.1. Western Mediterranean - Alboran Sea region

The input focal mechanisms from this region show a predominance of strike-slip, reverse faulting or mixed strike-slip/reverse (Fig. 7a). The median S_{Hmax} orientation in this region is 155°, in good agreement with the convergence direction between the Eurasia and the African plates at this location. The western part of this region (Gibraltar - south of Spain - Moroccan coast) has a relatively consistent S_{Hmax} orientation, except in the stress regions within the Alboran Sea. There, a rotation of >30° is observed and the elevated misfit angle β may signify increased stress heterogeneity (Fig. 7b). In contrast to this relatively consistent S_{Hmax}, the tectonic stress regime here is observed to rapidly change spatially. Reverse faulting is observed at the western border of the Betics Orogeny, signifying the elevated horizontal stresses to balance the gravitational potential energy from the topography and vice versa; at higher elevated areas within the Betics Orogeny normal faulting is prevailing. Along the African coast line, the S_{Hmax} orientation rotates gently rotates from N145°E to N168°E following the trend of the continental shelf. At the same time, the stress regime changes from strike-slip to reverse stress from west to east, reaching a high value for A_φ in the eastern coast of Algeria (Fig. 7c). There, a transpressional regime combining strike-slip and reverse faulting is observed in agreement with recent observations (Soumaya et al., 2018). A main set of fault structures running sub-parallel to the coast of Africa are nearly perpendicularly oriented with respect to the regional S_{Hmax} orientation. Median misfit angles tend to be $\beta < 20°$, except for near Oran in Algeria and for some of the inversions capturing the seismicity

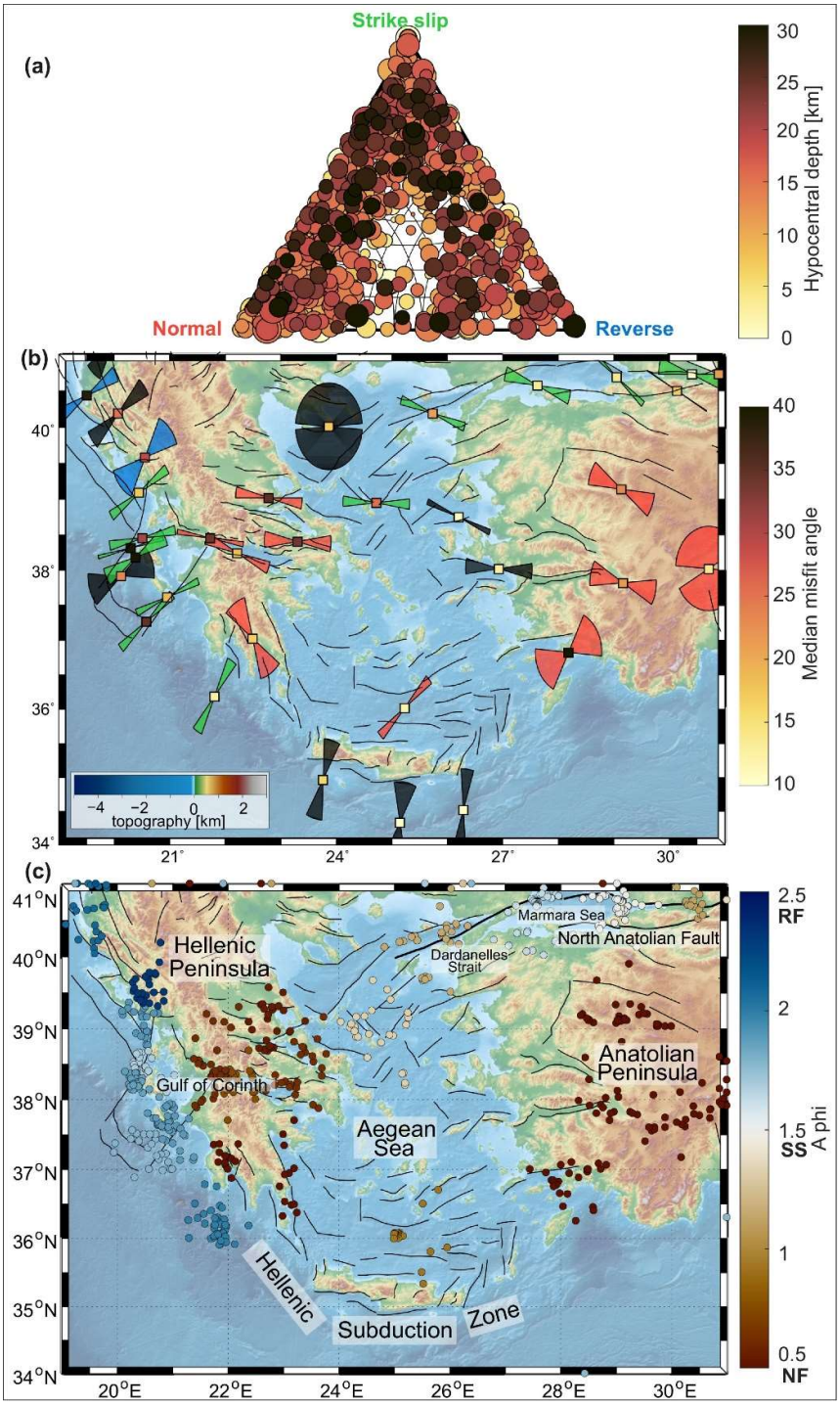

Figure 9. *Same as Fig. 7 but for eastern Mediterranean region.*

around the Al-Hoceima sequences (Fig. 7c). The elevated misfit angles from some of these small areas could be related e.g. to an increased focal mechanism variability of the aftershock sequences.

5.2. Central Mediterranean – Alpine Orogeny – Italian Peninsula

The central Mediterranean displays a complex tectonic and stress pattern as the result of the convergence point of several different geological units. The input focal mechanisms from this area indicate that the three faulting regimes (normal, strike-slip and reverse faulting) as well as numerous mechanisms displaying mixed regimes are present (Fig. 8a). The available catalog allowed to resolve in detail the stress part in the western part of the Alpine orogeny. Overall, the results from stress inversions surrounding the Alpine orogeny indicate a clockwise rotation from West to East of the S_{Hmax} orientation which is maintained roughly perpendicular to the main orogenic belt

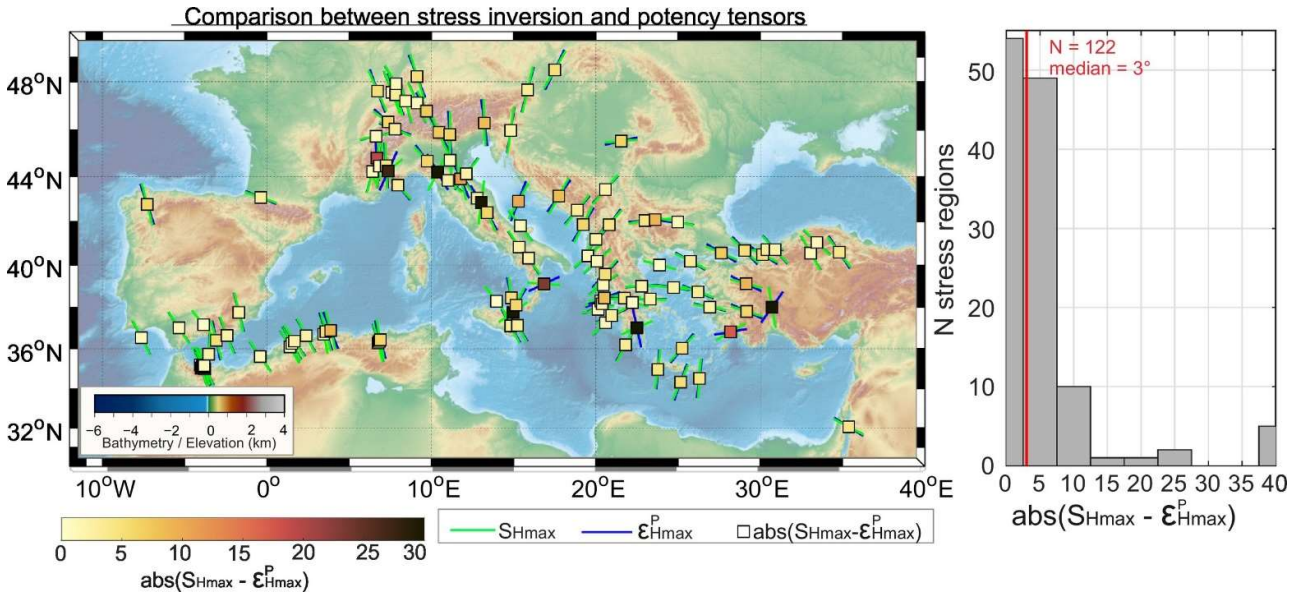

Figure 10. *Left: Map showing the maximum horizontal shortening orientation ($\varepsilon_{Hmax}{}^{P}$) derived from summation of normalized seismic potencies (blue lines) of the events within a stress region, together with the orientation of the maximum horizontal stress S_{Hmax} from the inversion of focal mechanisms (green lines). The color of the squares is encoded with the absolute difference between these two orientations. Right: Histogram displaying the distribution of absolute differences between these two orientations. (For interpretation of the references to color in this figure legend, the reader is referred to the web version of this article.)*

(Fig. 8b). In addition, increasing values for A_φ indicating a transition from normal stresses to strike-slip are observed within the Alpine orogeny from west to east (Fig. 8c). To the northwest of the Alps, a well-defined S_{Hmax} orientation of N151°E is recovered, which is oriented roughly perpendicular to the Alpine mountain range at this location. Similarly, a strike-slip stress regime with S_{Hmax} perpendicular to the Alpine range is recovered in the southern-central border. At these two regions, the stress regime appears to be a combination of strike-slip and transtensional. Since the overall depth of the seismicity from this region is comparable to that of the seismicity from the Betics orogeny (see Section 5.1), the magnitude of the horizontal stresses here is smaller than in the Betics orogeny. At the western border of the Alpine range, S_{Hmax} experience an anti-clockwise rotation following the shape of the orogenic belt, with a median recovered $S_{Hmax} = 32°$, although S_{Hmax} rapidly varies in space. As in the Betics, normal faulting is mainly observed below the orogeny, in agreement with enlarged vertical stress within the mountain range. A sharp increase of the A_φ value is observed in the southeastern border of the Alpine range, coinciding with the reverse fault that runs semi-parallel to the eastern coast of the Italian peninsula (Fig. 8). The majority of the median misfit angles tend to be $\beta < 30°$, except for some isolated stress inversions surrounding the Alpine orogeny and one stress inversion in the Tyrrhenian Sea.

Along the Italian Peninsula and in particular along the Apennines mountain range, S_{Hmax} is uniformly oriented N134°E (roughly coinciding with the strike of the mountain range), and normal faulting is prevailing (Fig. 8). The local normal faults that run along the Apennines mountain range appear to be well oriented for failure (i.e. about 30°) within the regional stress field orientation. However, a sharp change in the stress field orientation of about 90° occurs along the eastern coast of Italy and below the Adriatic Sea. There, the stress regime changes towards reverse faulting and S_{Hmax} is roughly oriented perpendicular to the coast, reflecting the collision of the Adriatic indenter with Eurasia along the Dinarides (Mantovani et al., 1990). Finally, the island of Sicily tends to display a S_{Hmax} orientation consistent with that of the Italian Peninsula (Fig. 8b). At this location, the A_φ values tend to be larger, reflecting mainly strike-slip tectonic regime and relatively larger horizontal stress magnitudes than in the Peninsula. However, the northeastern tip of the island appears to have an anomalous stress field, with S_{Hmax} oriented at N20°E and having a normal stress regime. This sharp stress rotation could be related with the different tectonic units that get in contact in this region (see e.g. Jolivet et al., 2013), or alternatively, related to the high topography of the active Etna volcano.

5.3. Eastern Mediterranean – Aegean – western Anatolian region

The eastern Mediterranean region including the Aegean subplate is characterized by a large rotation of S_{Hmax} which is maintained perpendicular to the Hellenic arc (Fig. 9). Focal mechanisms from this region indicate also the existence of the three faulting styles, and a relatively larger proportion of deep events (> 20 km) is apparent originating within the Benioff zone (Fig. 9a). Regions with the largest A_φ displaying transpressional and reverse stress regime are found along the eastern coast of Greece, following the Hellenic subduction zone. Within the Aegean subplate and in the eastern portion of Greece, a normal faulting stress regime with S_{Hmax} roughly oriented E-W is observed (Fig. 9b). Increased median misfit angles β

$< 30°$ appear around the Gulf of Corinth and some locations of the eastern part of the Hellenic Peninsula, possibly indicating larger stress heterogeneity or mixed stress regimes contained in these areas.

The North Anatolian Fault is a right-lateral transform fault separating the Anatolian and Eurasian plates. The plate-bounding fault runs as a strike-slip fault along most of its part. Its eastern end that is also the oldest portion with 13 Ma is at the Karliova triple junction in eastern Anatolia (e.g., Sengör, 2005) while its western end and the transition into the North Aegean is not very well defined (Armijo et al., 1999; Bohnhoff et al., 2016). We obtain a relatively stable strike-slip stress regime along the North Anatolian Fault and also from the eastern Sea of Marmara region to west of the Dardanelles strait in the west (North Aegean Sea). The median S_{Hmax} trend is N111°E. However, results from individual stress inversions in this region may deviate up to ±20° from this value in accordance with changes of the fault strike. This characteristic strike-slip stress field of the North Anatolian Fault is observed as far south as latitude 39° in the central Aegean Sea, which could suggest that the North Anatolian fault may extend at least until there (Fig. 9b). The majority of the median misfit angles $\beta < 20°$, suggesting relatively more homogeneous stresses here than in the Hellenic Peninsula.

Finally, the western portion of the Anatolian subplate is characterized by a north-south extensional normal faulting stress regime and remarkably low values for A_φ (Fig. 9b, c). This suggests that the magnitude of the vertical stress axis is remarkably larger than the magnitude of the two horizontal stresses, which, in turn, may result in a poorly defined trend of S_{Hmax}. Likely, this is the reason of the relatively large variety obtained for S_{Hmax} orientations in this region accompanied by larger uncertainties.

6. Comparison with strain observations and strain data

6.1. Derivation of coseismic strain from potency tensors

As introduced in Section 3, the stress and strain tensor orientations are only expected to coincide if: (1) the characteristic symmetry of the fault slip pattern is no less than orthorhombic, (2) the material is mechanically isotropic, (3) there is a linear constitutive relationship between the global stress and strain rates (Twiss and Unruh, 1998). Although stress field orientation is commonly inverted from earthquake focal mechanisms due to its relevance in seismology, focal mechanisms represent a measurement of the strain field.

To investigate how consistent the horizontal stress and strain field orientations are in the Mediterranean region, we resolved the coseismic strain pattern for each of our stress regions by summing the normalized seismic potency tensors (Ben-Zion and Zhu, 2002) of the seismic events contained within each region. The seismic potency density tensor can be calculated directly from the strike, dip and rake of the fault plane and it is defined as:

$$P_{ij} = \int_V \varepsilon_{ij}^P dV \tag{5}$$

where ε^P is the coseismic strain tensor, V is the source volume and i and j denote the three Cartesian directions (Ben-Zion, 2003, 2008). The orientation of the principal strain axes can be estimated from the normalized summation of earthquake potencies $\hat{P}_{ij}^{SM}$ in each of the regions (Bailey et al., 2009, 2010; Abolfathian et al., 2018). By employing potencies normalized to their scalar potency value, we can suppress the dominance of the largest events. The maximum horizontal shortening strain is then estimated following an analogous procedure as for the stress field (see Section 3).

In the majority of the studied regions, the orientation of the maximum horizontal (coseismic) shortening strain $\varepsilon_{Hmax}{}^P$ and the S_{Hmax} from our stress inversion are identical within error bounds, with a median difference of only 3° (Fig. 10). This suggests that in these regions, the stress and strain tensors are related with a linear constitutive law and that the other conditions from Twiss and Unruh, (1998) are also fulfilled. Only six regions out of the 122 studied here (reflecting only about 5% of the dataset) display differences larger than or equal to 25°. These isolated regions are located in the western Alpine orogeny, northern Apennines, Sicily, a small region in the Aegean, and northwestern Anatolia. Since for these inversions the stress and strain fields do not appear to coincide, the results from these six stress regions should be treated with caution.

6.2. Comparison with horizontal strain rate tensor from geodetic data

In the next step, we compare S_{Hmax} orientation from the stress inversion with the orientation of the maximum horizontal shortening strain-rate orientation at the surface ($\varepsilon_{Hmax}{}^G$), as derived from geodetic measurements. While the potency estimations discussed above only reflect the co-seismic portion of the strain tensor, the strain rate tensor derived from geodetic measurements is more representative of the strain rate tensor during the interseismic period. However, geodetic data can only capture the deformation at the surface, while both, stress inversion and potency tensors sample the formation at seismogenic depth.

We employed the Global Strain Rate Model (GSRM) data derived from integrating numerous GPS datasets at global scale (Kreemer et al., 2014). This data provides the orientation of the principal axes of the 2D horizontal strain rate tensor and the second invariant of the strain rate E_{II} on a regular 0.1° grid. The distribution of the $\varepsilon_{Hmax}{}^G$ trend from this model indicates approximately constant orientations around the entire western Mediterranean region as well as the Adriatic Sea, and a more heterogeneous pattern along Italy and the Anatolian Plate (Fig. S3a). The second invariant of the strain rate tensor clearly increases along the main active tectonic regions, i.e. along the North Anatolian Fault Zone and the Hellenic subduction zone. Increased second invariant of the strain rates are also observed along the Apennines in Italy and

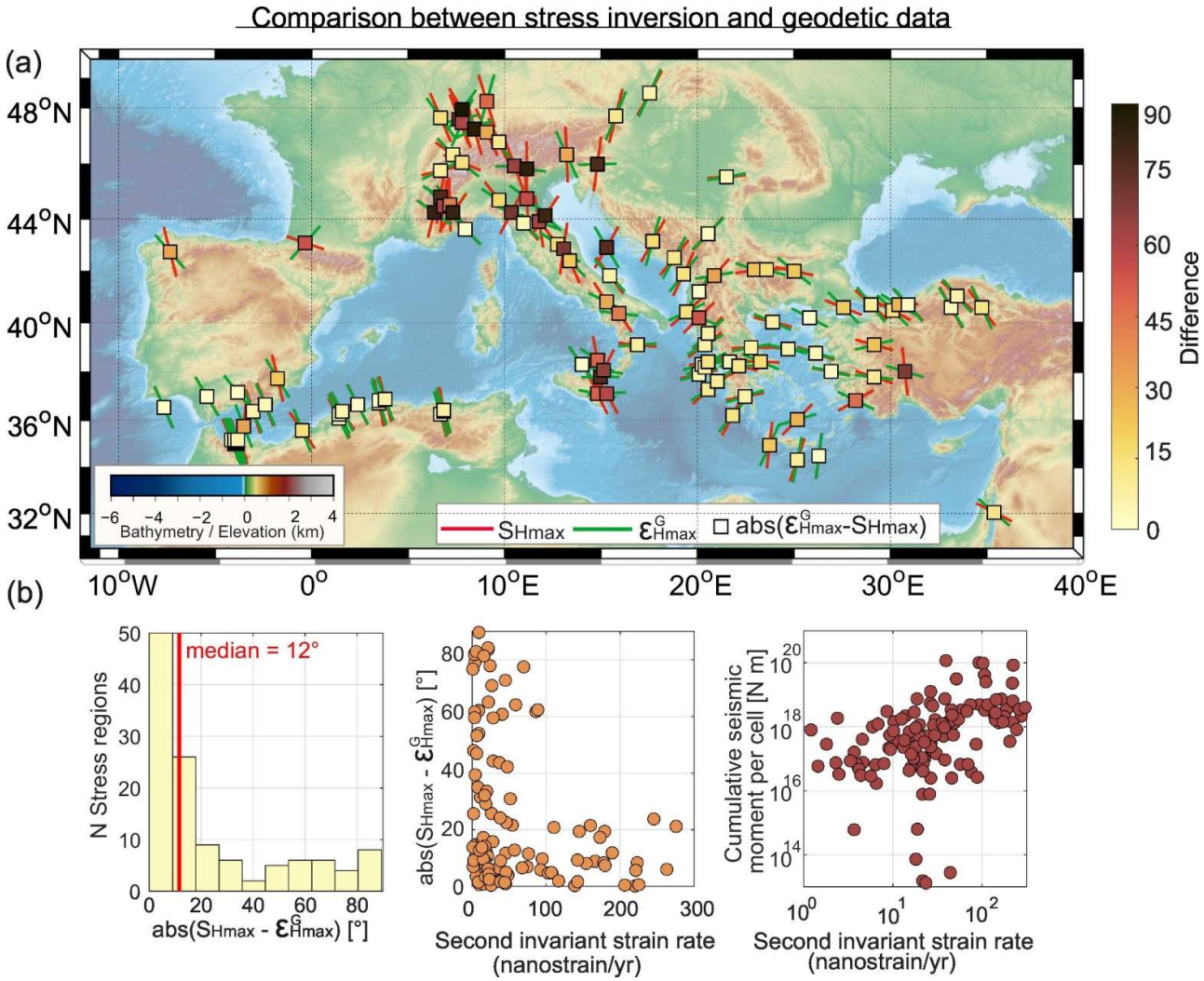

Figure 11. *(a) Map with the maximum horizontal stress orientation S_{Hmax} from stress inversion (red lines) and maximum shortening orientation $\varepsilon_{Hmax}{}^{G}$ from geodetic data (green lines). The square in the middle of the lines is encoded with the absolute difference between their orientations. (b) Different statistics showing the relation between S_{Hmax} from stress inversion, S_{Hmax} from stress2grid, $\varepsilon_{Hmax}{}^{G}$ and cumulative seismic moment ΣM0. From left to right: Histogram of differences between S_{Hmax} and $\varepsilon_{Hmax}{}^{G}$ orientations; differences between S_{Hmax} and $\varepsilon_{Hmax}{}^{G}$ orientations vs second invariant of the strain rate tensor; cumulative seismic moment release ΣM_0 per cell vs second invariant of the strain rate tensor. (For interpretation of the references to color in this figure legend, the reader is referred to the web version of this article.)*

at the Messina strait in northern Sicily (Fig. 8c, Fig. S3b).

For each stress region, we calculated the orientation of the largest horizontal shortening strain rate orientation $\varepsilon_{Hmax}{}^{G}$ and the second invariant of the strain rate tensor from the median values out of the 25 nearest GRSM grid points to the centroid of each corresponding region. Then, we estimated the absolute difference between the orientations of $\varepsilon_{Hmax}{}^{G}$ and S_{Hmax} from our stress inversion as previously done with the coseismic strain from potencies. The $\varepsilon_{Hmax}{}^{G}$ and S_{Hmax} orientations appear to be generally consistent at regional scale, with a median difference of 12° between them (Fig. 11a, b). This difference is larger than the median coseismic strain derived from summation of seismic potencies. Interestingly, the difference between $\varepsilon_{Hmax}{}^{G}$ and S_{Hmax} is generally <5° in the entire western Mediterranean as well as in the Anatolian Plate and the Aegean region, but they largely diverge in the central Mediterranean (i.e. Italian Peninsula) from the Alpine region to Sicily (Fig. 11a).

As the strain rate tensor can be better resolved when the second invariant is large, the second invariant of the strain rate tensor should be inversely proportional to the uncertainty of the strain rate tensor in that region. Accordingly, all regions from our study with a relatively large second invariant (> 100 nanostrain/yr) display a $abs(\varepsilon_{Hmax}{}^{G} - S_{Hmax}) < 20°$ (Fig. 11b). In addition, all regions with a greater difference between $\varepsilon_{Hmax}{}^{G}$ - S_{Hmax} are characterized with a second invariant <100 nanostrain/yr.

As in the Central Mediterranean region the second invariant tends to be relatively large (see Fig. S3b), the greater discrepancy of the orientations in central Mediterranean can only be partially explained by the resolution of the GSRM model. Interestingly, this region was also shown to display slightly larger differences between the stress and the coseismic strain from potency tensors. Therefore, it is possible that at this area, the strain field representing the entire interseismic period does not

entirely coincide with the background stress field driving the seismicity. Alternatively, the observed differences could in principle be caused by the different depth ranges sampled by the stress inversion and the geodetic data. In this sense, the largest stress rotations with depth are found in northern Italian Peninsula and Sicily, which are included here within the area where the $\varepsilon_{\mathrm{Hmax}}{}^{G}$ and S_{Hmax} differs the most. Fig. 11b (central panel) shows that the cumulative seismic moment release of each region tends to scale with the corresponding second invariant of the strain rate. This indicates that the regions with larger second invariant of the strain rate tend to be more seismically active.

In addition, we also compared the maximum horizontal shortening strain-rate orientation ($\varepsilon_{\mathrm{Hmax}}{}^{G}$) at the surface derived from the geodetic data with the maximum horizontal stress derived using the mean S_{Hmax} orientation on the regular grid based on all stress data with A-C quality from the WSM database release 2016 except those from single focal mechanisms. Interestingly, increased discrepancies are observed, with a median difference of 40° between both of them (Fig. S4). Only a few locations appear to have small differences between these orientations, in particular the Iberian Peninsula, the southern portion of the Italian Peninsula (excluding Sicily) and the southern portion of the Corinth Gulf. These increased differences possibly highlight a non-simple relation between stress and strain rate near the surface.

7. Conclusions

In this study, we mapped the stress field orientation and related parameters in the Mediterranean region employing focal mechanism data from the WSM database release 2016. We utilized a parameter-free technique which allowed us to achieve a higher resolution than previous studies. Our main conclusions are as follows:

1) The here applied stress inversion methodology is successfully capturing the main regional features of the stress field orientation even in a tectonically complex region as the Mediterranean, and it is capable of resolving also local features such as larger lateral heterogeneity when the available data is sufficient.
2) S_{Hmax} orientations derived from our stress inversions tend to be uniform with depth within uncertainties. However, a trend of decreasing stress heterogeneity with increasing depth is recovered from 5 to 14 km to 21-30 km. The trend is recovered by means of the focal mechanism variability as well as the misfit angle between stress field orientations and slip vectors from individual mechanisms.
3) Our stress inversion results are consistent with those that integrate all WSM data records. Regions with increased discrepancy are small regions near the Adriatic Sea, along the western North Anatolian Fault Zone and the western portion of the Alpine orogeny. The increased difference between the inversion and other indicators may represent larger stress heterogeneity in these regions, between very shallow depth (e.g.<5 km) sampled by borehole breakouts) and seismogenic depth (sampled by focal mechanisms).
4) Both the coseismic elastic strain field derived from summation of potency tensors and the horizontal strain rate tensor from GPS data are highly consistent with the co-seismic stress field orientation in the brittle crust. This indicates that in the studied region, stress and strain fields maintain a linear relationship and that co-seismic strain release tends to be generally consistent with the interseismic strain accumulation. Furthermore, this suggests that at this region, plate boundary forces (e.g. the plate motion) play a key control on the orientation of the stress tensor. A notorious exception is the central Mediterranean region, including the Alpine Orogeny, Italian Peninsula and the island of Sicily, where larger discrepancies are found.

Supplementary data to this article can be found online at https://doi.org/10.1016/j.tecto.2019.228286.

Author's contribution

Patricia Martínez-Garzón: Conceptualization, Formal analysis, Funding acquisition, Investigation; Methodology; Manuscript writing and reviewing.

Oliver Heidbach: Data curation; Investigation; Manuscript writing and reviewing.

Marco Bohnhoff: Funding acquisition; Investigation; Methodology; Manuscript writing and reviewing.

Declaration of competing interest

The authors have no interests to declare.

Acknowledgements

We thank Claudia Piromallo, an anonymous reviewer and the Editor Philippe Agard for providing constructive feedback which substantially improved the paper. PMG acknowledges funding from the Helmholtz Association in the frame of the Young Investigators Group VH-NG-1232 (SAIDAN). Focal mechanism data from this study is publicly available through the WSM database release 2016 (Heidbach et al., 2018). Strain rates and orientation of the strain field from GPS data corresponds to the GSRM model described in Kreemer et al. (2014). We appreciate the feedback from Corné Kreemer in handling and utilizing the strain rate data. Fruitful discussions with Yehuda Ben-Zion and Georg Dresen are acknowledged.

References

Abolfathian, N., Martínez-Garzón, P., Ben-Zion, Y., 2018. Spatiotemporal variations of stress and strain parameters in the San Jacinto fault zone. Pure Appl. Geophys. https://doi.org/10.1007/s00024-018-2055-y.

Anderson, E.M., 1951. The dynamics of faulting and dyke formation with applications to Britain. Houston, Texas: Hafner Pub. Co.

Assumpção, M., Dias, F.L., Zevallos, I., Naliboff, J.B., 2016. Intraplate stress field in South America from earthquake focal mechanisms. J. S. Am. Earth Sci. 71, 278-295. https://doi.org/10.1016/j.jsames.2016.07.005.

Armijo, R., Meyer, B., Hubert, A., Barka, A., 1999. Westward propagation of the North Anatolian fault into the northern Aegean. Timing and kinematics. Geology 27 (3), 267-270. https://doi.org/10.1130/0091-7613(1999)027<0267:WPOTNA>2.3.CO;2.

Bailey, I.W., Becker, T.W., Ben-Zion, Y., 2009. Patterns of co-seismic strain computed from southern California focal mechanisms. Geophys. J. Int. 177, 1015-1036. https://doi.org/10.1111/j.1365-246X.2009.

04090.x.
Bailey, I.W., Ben-Zion, Y., Becker, T.W., Holschneider, M., 2010. Quantifying focal mechanism heterogeneity for fault zones in central and southern California. Geophys. J. Int. 183, 433-450. https://doi.org/10.1111/j.1365-246X.2010.04745.x.
Ben-Zion, Y., 2003. Appendix 2 Key formulas in earthquake seismology, in: William H.K. Lee, H.K., Paul C. Jennings and Carl Kisslinger (Ed.), International Geophysics. Academic Press, pp. 1857-1875.
Ben-Zion, Y., 2008. Collective behavior of earthquakes and faults: continuum-discrete transitions, progressive evolutionary changes, and different dynamic regimes. Rev. Geophys. 46, RG4006. https://doi.org/10.1029/2008RG000260.
Ben-Zion, Y., Zhu, L., 2002. Potency-magnitude scaling relations for southern California earthquakes with 1.0<ML<7.0. Geophys. J. Int. 148, F1-F5. https://doi.org/10.1046/j.1365-246X.2002.01637.x.
Bird, P., Ben-Avraham, Z., Schubert, G., Andreoli, M., Viola, G., 2006. Patterns of stress and strain rate in southern Africa. J. Geophys. Res. Solid Earth 111. https://doi.org/10.1029/2005JB003882.
Bohnhoff, M., Harjes, H.-P., Meier, T., 2005. Deformation and stress regimes in the Hellenic subduction zone from focal Mechanisms. J. Seismol. 9, 341-366. https://doi.org/10.1007/s10950-005-8720-5.
Bohnhoff, M., Martínez-Garzón, P., Bulut, F., Stierle, E., Ben-Zion, Y., 2016. Maximum earthquake magnitudes along different sections of the North Anatolian fault zone. Tectonophysics 674, 147-165. https://doi.org/10.1016/j.tecto.2016.02.028.
Brudy, M., Zoback, M.D., Fuchs, K., Rummel, F., Baumgärtner, J., 1997. Estimation of the complete stress tensor to 8 km depth in the KTB scientific drill holes: Implications for crustal strength. J. Geophys. Res. Solid Earth 102, 18453-18475. https://doi.org/10.1029/96JB02942.
Carafa, M.M.C., Barba, S., 2013. The stress field in Europe: optimal orientations with confidence limits. Geophysical Journal International 193 (2), 531-548. https://doi.org/10.1093/gji/ggt024.
Célérier B., B., 2010. Remarks on the relationship between the tectonic regime, the rake of the slip vectors, the dip of the nodal planes, and the plunges of the P, B, and T axes of earthquake focal mechanisms. Tectonophysics, Frontiers in Stress Research 482, 42-49. https://doi.org/10.1016/j.tecto.2009.03.006.
Cloetingh, S.A.P.L., Ziegler, P.A., Bogaard, P.J.F., Andriessen, P.A.M., Artemieva, I.M., Bada, G., van Balen, R.T., Beekman, F., Ben-Avraham, Z., Brun, J.-P., Bunge, H.P., Burov, E.B., Carbonell, R., Faccenna, C., Friedrich, A., Gallart, J., Green, A.G., Heidbach, O., Jones, A.G., Matenco, L., Mosar, J., Oncken, O., Pascal, C., Peters, G., Sliaupa, S., Soesoo, A., Spakman, W., Stephenson, R.A., Thybo, H., Torsvik, T., de Vicente, G., Wenzel, F., Wortel, M.J.R., 2007. TOPO-EUROPE: the geoscience of coupled deep Earth-surface processes. Global and Planetary Change, TOPO-EUROPE: the Geoscience of Coupled Deep Earth-Surface Processes 58, 1-118. https://doi.org/10.1016/j.gloplacha.2007.02.008.
Custódio, S., Lima, V., Vales, D., Cesca, S., Carrilho, F., 2016. Imaging active faulting in a region of distributed deformation from the joint clustering of focal mechanisms and hypocentres: Application to the Azores-western Mediterranean region. Tectonophysics 676, 70-89. https://doi.org/10.1016/j.tecto.2016.03.013.
Fernández-Ibáñez, F., Soto, J.I., Zoback, M.D., Morales, J., 2007. Present-day stress field in the Gibraltar Arc (western Mediterranean). J. Geophys. Res. Solid Earth 112. https://doi.org/10.1029/2006JB004683.
Frepoli, A., Amato, A., 2000. Spatial variation in stresses in peninsular Italy and Sicily from background seismicity. Tectonophysics 317, 109-124. https://doi.org/10.1016/S0040-1951(99)00265-6.
Ghisetti, F., 2000. Slip partitioning and deformation cycles close to major faults in southern California: evidence from small-scale faults. Tectonics 19, 25-43. https://doi.org/10.1029/1999TC900054.
Giardini, D., Wössner, J., Danciu, L., 2014. Mapping Europe's seismic hazard. Eos. Trans. AGU 95, 261-262. https://doi.org/10.1002/2014EO290001.
Gölke, M., Coblentz, D., 1996. Origins of the European regional stress field. Tectonophysics, Dynamics of Extensional Basins and Inversion Tectonics 266, 11-24. https://doi.org/10.1016/S0040-1951(96)00180-1.
Grünthal, G., Wahlström, R., 2012. The European-Mediterranean Earthquake Catalogue (EMEC) for the last millennium. J. Seismol. 16 (3), 535-570. https://doi.org/10.1007/s10950-012-9302-y.
Hardebeck, J.L., Hauksson, E., 2001. Crustal stress field in southern California and its implications for fault mechanics. J. Geophys. Res. 106, 21859-21882. https://doi.org/10.1029/2001JB000292.
Hardebeck, J.L., Michael, A.J., 2006. Damped regional-scale stress inversions: methodology and examples for southern California and the Coalinga aftershock sequence. J. Geophys. Res. Solid Earth 111, B11310. https://doi.org/10.1029/2005JB004144.
Heidbach, O., Ben-Avraham, Z., 2007. Stress evolution and seismic hazard of the Dead Sea Fault System. Earth Planet. Sci. Lett. 257, 299-312. https://doi.org/10.1016/j.epsl.2007.02.042.
Heidbach, O., Drewes, H., 2003. 3-D Finite Element model of major tectonic processes in the Eastern Mediterranean. In: Nieuwland, D. (Ed.), New Insigths in Structural Interpretation and Modelling. Spec. Publs. Geol. Soc, London, pp. 261-274. https://doi.org/10.1144/GSL.SP.2003.212.01.17.
Heidbach, O., Tingay, M., Barth, A., Reinecker, J., Kurfeß, D., Müller, B., 2010. Global crustal stress pattern based on the World Stress Map database release 2008. Tectonophysics 482, 3-15. https://doi.org/10.1016/j.tecto.2009.07.023.
Heidbach, O., Rajabi, M., Cui, X., Fuchs, K., Müller, B., Reinecker, J., Reiter, K., Tingay, M., Wenzel, F., Xie, F., Ziegler, M.O., Zoback, M.-L., Zoback, M., 2018. The World Stress Map database release 2016: crustal stress pattern across scales. Tectonophysics 744, 484-498. https://doi.org/10.1016/j.tecto.2018.07.007.
Hergert, T., Heidbach, O., 2010. Slip-rate variability and distributed deformation in the Marmara Sea fault system. Nat. Geosci. 3, 132-135. https://doi.org/10.1038/ngeo739.
Houlié, N., Woessner, J., Giardini, D., Rothacher, M., 2018. Lithosphere strain rate and stress field orientations near the Alpine arc in Switzerland. Sci. Rep. 8, 2018. https://doi.org/10.1038/s41598-018-20253-z.
Hu, X., Zang, A., Heidbach, O., Cui, X., Xie, F., Chen, J., 2017. Crustal stress pattern in China and its adjacent areas. Journal of Asian Earth Sciences, Tectonics, Volcanism and Geo-energy in East Asia 149, 20-28. https://doi.org/10.1016/j.jseaes.2017.07.005.
Hurd, Owen, Zoback, M.D., 2012. Regional stress orientations and slip compatibility of earthquake focal planes in the New Madrid seismic zone. Seismol. Res. Lett. 83, 672-679. https://doi.org/10.1785/0220110122.
Jolivet, L., Faccenna, C., Piromallo, C., 2009. From mantle to crust: stretching the Mediterranean. Earth Planet. Sci. Lett. 285, 198-209. https://doi.org/10.1016/j.epsl.2009.06.017.
Jolivet, L., Faccenna, C., Huet, B., Labrousse, L., Le Pourhiet, L., Lacombe, O., Lecomte, E., Burov, E., Denèle, Y., Brun, J.-P., Philippon, M., Paul, A., Salaün, G., Karabulut, H., Piromallo, C., Monié, P., Gueydan, F., Okay, A.I., Oberhänsli, R., Pourteau, A., Augier, R., Gadenne, L., Driussi, O., 2013. Aegean tectonics: strain localisation, slab tearing and trench retreat. Tectonophysics 597-598, 1-33. https://doi.org/10.1016/j.tecto.2012.06.011. The Aegean: a natural laboratory for tectonics - Neotectonics.
Kagan, Y.Y., 1991. 3-D rotation of double-couple earthquake sources. Geophys. J. Int. 106, 709-716.
Kastrup, U., Zoback, M.L., Deichmann, N., Evans, K.F., Giardini, D., Michael, A.J., 2004. Stress field variations in the Swiss Alps and the northern Alpine foreland derived from inversion of fault plane solutions. J. Geophys. Res. Solid Earth 109. https://doi.org/10.1029/2003JB002550.
Kiratzi, A.A., 2002. Stress tensor inversions along the westernmost North Anatolian Fault Zone and its continuation into the North Aegean Sea. Geophys. J. Int. 151, 360-376. https://doi.org/10.1046/j.1365-246X.2002.01753.x.
Konstantinou, K.I., Mouslopoulou, V., Liang, W.-T., Heidbach, O., Oncken, O., Suppe, J., 2017. Present-day crustal stress field in Greece inferred from regional-scale damped inversion of earthquake focal mechanisms. J. Geophys. Res. Solid Earth. https://doi.org/10.1002/2016JB013272. (2016JB013272).
Kreemer, C., Chamot-Rooke, N., 2004. Contemporary kinematics of the southern Aegean and the Mediterranean Ridge. Geophys. J. Int. 157 (3), 1377-1392. https://doi.org/10.1111/j.1365-246X.2004.02270.x.
Kreemer, C., Blewitt, G., Klein, E.C., 2014. A geodetic plate motion and Global Strain Rate Model. Geochem. Geophys. Geosyst. 15, 3849-3889. https://doi.org/10.1002/2014GC005407.
Le Pichon, X., Kreemer, C., 2010. The Miocene-to-Present kinematic evolution of the eastern Mediterranean and Middle East and its implications for dynamics. Annu. Rev. Earth Planet. Sci. 38 (1), 323-351. https://doi.org/10.1146/annurev-earth-040809-152419.
Lund, B., Townend, J., 2007. Calculating horizontal stress orientations with full or partial knowledge of the tectonic stress tensor. Geophys. J. Int. 170, 1328-1335. https://doi.org/10.1111/j.1365-246X.2007.03468.x.

Luttrell, K., Smith-Konter, B., 2017. Limits on crustal differential stress in southern California from topography and earthquake focal mechanisms. Geophys. J. Int. 211, 472-482. https://doi.org/10.1093/gji/ggx301.

Mantovani, E., Babbucci, D., Albarello, D., Mucciarelli, M., 1990. Deformation pattern in the central Mediterranean and behavior of the African/Adriatic promontory. Tectonophysics 179, 63-79. https://doi.org/10.1016/0040-1951(90)90356-D. Seismicity and Crustal Deformation.

Martínez‐Garzón, P., Kwiatek, G., Ickrath, M., Kwiatek, G., Bohnhoff, M., 2014. MSATSI: A MATLAB Package for Stress Inversion Combining Solid Classic Methodology, a New Simplified User‐Handling, and a Visualization Tool. Seismological Research Letters 85 (4), 896-904. https://doi.org/10.1785/0220130189.

Martínez-Garzón, P., Kwiatek, G., Bohnhoff, M., Dresen, G., 2016a. Impact of fluid injection on fracture reactivation at The Geysers geothermal field. J. Geophys. Res. 121. https://doi.org/10.1002/2016JB013137.

Martínez-Garzón, P., Ben-Zion, Y., Abolfathian, N., Kwiatek, G., Bohnhoff, M., 2016b. A refined methodology for stress inversions of earthquake focal mechanisms. J. Geophys. Res. Solid Earth 121, 8666-8687. https://doi.org/10.1002/2016JB013493.

McClusky, S., Balassanian, S., Barka, A., Demir, C., Ergintav, S., Georgiev, I., Gurkan, O., Hamburger, M., Hurst, K., Kahle, H., Kastens, K., Kekelidze, G., King, R., Kotzev, V., Lenk, O., Mahmoud, S., Mishin, A., Nadariya, M., Ouzounis, A., Paradissis, D., Peter, Y., Prilepin, M., Reilinger, R., Sanli, I., Seeger, H., Tealeb, A., Toksöz, M.N., Veis, G., 2000. Global Positioning System constraints on plate kinematics and dynamics in the eastern Mediterranean and Caucasus. J. Geophys. Res. 105, 5695-5719. https://doi.org/10.1029/1999JB900351.

McClusky, S., Reilinger, R., Mahmoud, S., Sari, D.B., Tealab, A., 2003. GPS constraints on Africa (Nubia) and Arabia plate motions. Geophys. J. Int. 155, 126-138.

McKenzie, D.P., 1969. The relation between fault plane solutions for earthquakes and the directions of the principal stresses. Bull. Seismol. Soc. Am. 59, 591-601.

Michael, A.J., 1984. Determination of stress from slip data: faults and folds. J. Geophys. Res. Solid Earth 89, 11517-11526. https://doi.org/10.1029/JB089iB13p11517.

Michael, A.J., 1987. Use of focal mechanisms to determine stress: a control study. J. Geophys. Res. Solid Earth 92, 357-368. https://doi.org/10.1029/JB092iB01p00357.

Montone, P., Mariucci, M.T., Pondrelli, S., Amato, A., 2004. An improved stress map for Italy and surrounding regions (central Mediterranean). J. Geophys. Res. Solid Earth 109. https://doi.org/10.1029/2003JB002703.

Morris, A., Ferrill, D.A., Henderson, D.B., 1996. Slip-tendency analysis and fault reactivation. Geology 24, 275-278. https://doi.org/10.1130/0091-7613(1996)024<0275:STAAFR>2.3.CO;2.

Müller, B., Zoback, M.L., Fuchs, K., Mastin, L., Gregersen, S., Pavoni, N., Stephansson, O., Ljunggren, C., 1992. Regional patterns of tectonic stress in Europe. J. Geophys. Res. Solid Earth 97, 11783-11803. https://doi.org/10.1029/91JB01096.

Örgülü, G., 2011. Seismicity and source parameters for small-scale earthquakes along the splays of the North Anatolian Fault (NAF) in the Marmara Sea. Geophys. J. Int. 184, 385-404. https://doi.org/10.1111/j.1365-246X.2010.04844.x.

Ousadou, F., Dorbath, L., Ayadi, A., Dorbath, C., Gharbi, S., 2014. Stress field variations along the Maghreb region derived from inversion of major seismic crisis fault plane solutions. Tectonophysics 632, 261-280. https://doi.org/10.1016/j.tecto.2014.06.017.

Pierdominici, S., Heidbach, O., 2012. Stress field of Italy − mean stress orientation at different depths and wave-length of the stress pattern. Tectonophysics 532-535, 301-311. https://doi.org/10.1016/j.tecto.2012.02.018.

Rajabi, M., Tingay, M., Heidbach, O., Hillis, R., Reynolds, S., 2017. The present-day stress field of Australia. Earth Sci. Rev. 168, 165-189. https://doi.org/10.1016/j.earscirev.2017.04.003.

Rebaï, S., Philip, H., Taboada, A., 1992. Modern tectonic stress field in the Mediterranean region: evidence for variation in stress directions at different scales. Geophys. J. Int. 110, 106-140. https://doi.org/10.1111/j.1365-246X.1992.tb00717.x.

Reilinger, R., McClusky, S., Vernant, P., Lawrence, S., Ergintav, S., Cakmak, R., Ozener, H., Kadirov, F., Guliev, I., Stepanyan, R., Nadariya, M., Hahubia, G., Mahmoud, S., Sakr, K., ArRajehi, A., Paradissis, D., Al-Aydrus, A., Prilepin, M., Guseva, T., Evren, E., Dmitrotsa, A., Filikov, S.V., Gomez, F., Al-Ghazzi, R., Karam, G., 2006. GPS constraints on continental deformation in the Africa-Arabia-Eurasia continental collision zone and implications for the dynamics of plate interactions. J. Geophys. Res. 111, B05411. https://doi.org/10.1029/2005JB004051.

Reinecker, J., Tingay, M., Müller, B., Heidbach, O., 2010. Present-day stress orientation in the Molasse Basin. Tectonophysics 482, 129-138. https://doi.org/10.1016/j.tecto.2009.07.021.

Reiter, K., Heidbach, O., Schmitt, D., Haug, K., Ziegler, M., Moeck, I., 2014. A revised crustal stress orientation database for Canada. Tectonophysics 636, 111-124. https://doi.org/10.1016/j.tecto.2014.08.006.

Richardson, R.M., 1992. Ridge forces, absolute plate motions, and the intraplate stress field. J. Geophys. Res. 97, 11739-11748.

Scheidegger, A.E., 1981. The stress-field in the alpine-mediterranean region. Geophys. Surv. 4, 233-253. https://doi.org/10.1007/BF01449186.

Scholz, C.H., 2002. The Mechanics of Earthquakes and Faulting, 2nd ed. Cambridge University Press.

Sengör, A.M.C., 2005. The North Anatolian Fault: a new look. Ann. Rev. Earth Panet. Sci. 33, 37-112.

Simpson, R.W., 1997. Quantifying Anderson's fault types. J. Geophys. Res. 102, 17909-17919. https://doi.org/10.1029/97JB01274.

Soumaya, A., Ben Ayed, N., Rajabi, M., Meghraoui, M., Delvaux, D., Kadri, A., Ziegler, M., Maouche, S., Braham, A., 2018. Active Faulting geometry and stress pattern near complex strike-slip systems along the Maghreb region: constraints on active convergence in the western Mediterranean. Tectonics 37, 3148-3173. https://doi.org/10.1029/2018TC004983.

Spakman, W., Chertova, M.V., Berg, A. van den, Hinsbergen, D.J.J. van, 2018. Puzzling features of western Mediterranean tectonics explained by slab dragging. Nat. Geosci. 11, 211-216. https://doi.org/10.1038/s41561-018-0066-z.

Stein, R.S., Barka, A.A., Dieterich, J.H., 1997. Progressive failure on the North Anatolian fault since 1939 by earthquake stress triggering. Geophys. J. Int. 128, 594-604. https://doi.org/10.1111/j.1365-246X.1997.tb05321.x.

Twiss, R.J., Unruh, J.R., 1998. Analysis of fault slip inversions: do they constrain stress or strain rate? J. Geophys. Res. 103, 12205-12222. https://doi.org/10.1029/98JB00612.

Vavryčuk, V., 2011. Principal earthquakes: Theory and observations for the 2008 West Bohemia swarm. Earth Planet. Sci. Lett. 305, 290-296. https://doi.org/10.1016/j.epsl.2011.03.002.

Vavryčuk, V., 2014. Iterative joint inversion for stress and fault orientations from focal mechanisms. Geophys. J. Int. 199, 69-77. https://doi.org/10.1093/gji/ggu224.

Wallace, R.E., 1951. Geometry of shearing stress and relation to faulting. J. Geol. 59, 118-130.

Walsh, F.R., Zoback, M.D., 2016. Probabilistic assessment of potential fault slip related to injection-induced earthquakes: application to north-central Oklahoma, USA. Geology 44, 991-994. https://doi.org/10.1130/G38275.1.

Westaway, R., 1994. Present-day kinematics of the Middle East and eastern Mediterranean. J. Geophys. Res. 99, 12071-12090. https://doi.org/10.1029/94JB00335.

Wollin, C., Bohnhoff, M., Vavryčuk, V., Martínez-Garzón, P., 2018. Stress inversion of regional seismicity in the Sea of Marmara region, Turkey. Pure Appl. Geophys. https://doi.org/10.1007/s00024-018-1971-1.

Ziegler, M., Heidbach, O., 2019. Manual of the Matlab Script Stress2Grid v1.1, WSM Technical Report 19-02. GFZ German Research Centre for Geoscienceshttps://doi.org/10.2312/wsm.2019.002. 33 p.

Zoback, M.L., 1992. First- and second-order patterns of stress in the lithosphere: the World Stress Map Project. J. Geophys. Res. Solid Earth 97, 11703-11728. https://doi.org/10.1029/92JB00132.

Zoback, M.L., Zoback, M.D., Adams, J., Assumpção, M., Bell, S., Bergman, E.A., Blümling, P., Brereton, N.R., Denham, D., Ding, J., Fuchs, K., Gay, N., Gregersen, S., Gupta, H.K., Gvishiani, A., Jacob, K., Klein, R., Knoll, P., Magee, M., Mercier, J.L., Müller, B.C., Paquin, C., Rajendran, K., Stephansson, O., Suarez, G., Suter, M., Udias, A., Xu, Z.H., Zhizhin, M., 1989. Global patterns of tectonic stress. Nature 341, 291-298. https://doi.org/10.1038/341291a0.